Int. J. Multiphase Flow Vol. 18, No. 6, pp. 891–903, 1992
Printed in Great Britain.

0301-9322/92 $5.00 + 0.00

MEASUREMENTS AND SIMULATIONS OF PARTICLE DISPERSION IN A TURBULENT FLOW

C. J. CALL and I. M. KENNEDY
Department of Mechanical, Aeronautical, and Materials Engineering, University of California, Davis, CA 95616, U.S.A.

(Received 12 July 1991; in revised form 24 June 1992)

Abstract—A particle imaging technique has been used to collect droplet displacement statistics in a round turbulent jet of air. Droplets are injected on the jet axis, and a laser sheet and position-sensitive photomultiplier tube are used to track their radial displacement and time-of-flight. Dispersion statistics can be computed which are Lagrangian or Eulerian in nature. The experiments have been simulated numerically using a second-order closure scheme for the jet and a stochastic simulation for the particle trajectories. Results are presented for non-vaporizing droplets of sizes from 35 to 160 μm. The simulations have underscored the importance of initial conditions and early droplet displacement history on the droplet trajectory for droplets with large inertia relative to the turbulence. Estimates of initial conditions have been made and their effect on dispersion is quantified.

Key Words: particle dispersion, shear flow, droplets, stochastic simulation

1. INTRODUCTION

Liquid sprays are widely utilized in our society for energy production, application of coatings and waste incineration. Increasingly, designers of spray systems employ computers for the numerical simulations of sprays in the development of improved devices. The numerical problem is complex and today's "state-of-the-art" spray simulations are somewhat crude. Continued improvement of spray models requires experimental measurements obtained in well-characterized turbulent flows, since turbulence plays an important role in the transport process. The objective of this study is to improve our understanding or turbulence particle dispersion.

The classical study of turbulent dispersion of a fluid particle was that of Taylor (1921). The fundamental result gives the mean square particle displacement, or dispersion, in homogeneous turbulence in terms of a Lagrangian fluid particle autocorrelation:

$$\sigma^2_{f,x_2}(t) = 2\int_0^t \int_0^{t'} \langle v^2_{f,x_2}(t)\rangle^{1/2}\langle v^2_{f,x_2}(t')\rangle^{1/2} R^L_{f,x_2}(t,t')\,dt'\,dt, \quad [1]$$

where the dispersion is, by definition, the mean square displacement in the direction x_2 from a point source and where the autocorrelation function R^L_{f,x_2} is defined by

$$R^L_{f,x_2}(t,t') = \frac{\langle v^2_{f,x_2}(t) v^2_{f,x_2}(t')\rangle}{\langle v^2_{f,x_2}(t)\rangle^{1/2}\langle v^2_{f,x_2}(t')\rangle^{1/2}}, \quad [2]$$

where $t' = t + \theta$, with θ being the lag or separation time of the correlation. Displacement is a random variable, and averages refer to ensembles of realizations of the variable at time t or t'. The statistically average fluid particle velocity, $\langle v^2_{f,x_2}\rangle^{1/2}$, is constant in time for flows stationary in the Lagrangian frame. As a constant, it can be written outside of the integrals of [1]. Snyder & Lumley (1971) pointed out that these equations can be applied to discrete particles with the appropriate definition of R^L_{p,x_2} based on the velocity correlation of the discrete particle. Direct use of the theory requires knowledge of the particle's Lagrangian autocorrelation function, which is generally unknown.

Although the theory is not directly applicable to more practical flows such a round jet, it does provide a framework for the interpretation of measurements. A special case of Taylor's theory is of interest here. For short times-of-flight (i.e. near the point of particle release), the particle velocity

is perfectly correlated with itself: $t = 0$, $t' \to 0$ such that $R^1_{p,x_2}(0, t') \cong 1$. Equation [1] can be integrated with $\langle v^2_{p,x_2}(0)\rangle = \langle v^2_{p,x_2}(t')\rangle$, and the dispersion is quadratic in time:

$$\sigma^2_{p,x_2} = \langle v^2_{p,x_2}(0)\rangle t^2 \quad \text{(small } t\text{)}. \qquad [3]$$

For large separation times, the particle diffusivity ε_{p,x_2}, commonly defined by $\frac{1}{2}\,\mathrm{d}\sigma^2_{p,x_2}/\mathrm{d}t$, is constant in stationary flows.

Most measurements of round jet dispersion presented in the literature are of the Eulerian type, i.e. the data is obtained solely in the spatial domain. For example, Yuu *et al.* (1978) studied a turbulent round jet which was seeded with fly ash. Using an isokinetic sampling probe they measured mean particle fluxes. Recently, Hardalupas *et al.* (1989) have undertaken an investigation of particle flux and velocity statistics in a round jet (for $x_1/D < 30$) seeded with round glass beads. The objective was to quantify the effects of mass loading and particle size on mean and r.m.s. velocities of the gas and particle phase and the particle axial mass flux.

Measurements such as these may not be ideal for use in the development of spray models. Lagrangian statistics are fundamentally more relevant in developing spray models, which rely on the integration of particle equations of motion. Two studies in which Lagrangian measurements are presented are noted here. Snyder & Lumley (1971) performed a classic experiment on solid particle dispersion in quasi-homogeneous grid turbulence. Direct measurements of the Lagrangian particle velocity correlation and the dispersion rate were presented. Transformations were applied to compensate for turbulence decay so that the fluctuations were stationary. Measurements were not obtained near the particle injector. Vames & Hanratty (1988) have used a particle counter to provide essentially Lagrangian dispersion measurements of dispersion for droplets in isothermal pipe turbulence. The objective was to compare particle and fluid turbulence properties.

These types of experiments are directly useful and relevant for the validation of spray models which are based on the integration of single particle trajectories. This widely used approach, proposed by Gosman & Ioannides (1981), relies on a random number generator to choose "eddy lifetimes" subject to some distribution. A number of researchers have since used this simulation technique (e.g. Shuen *et al.* 1983; Solomon *et al.* 1985a, b; Chen & Crowe 1984), and some are reviewed by Faeth (1987) and Crowe *et al.* (1988). However, the initial conditions need to be prescribed, as pointed out by Berlemont *et al.* (1990). They observed that much of the available data on droplet dispersion does not include the initial conditions required by stochastic simulations.

The study by Solomon *et al.* (1985a) investigated a spray formed with an air-atomized injector. In their stochastic simulation, they found it was necessary to estimate initial conditions for the droplets from measurements obtained at $x_1/D = 50$ in order to avoid the effects of liquid ligaments near the injector.

This paper presents experimental measurements and numerical simulations of droplet dispersion within an isothermal round jet shear flow. The measurements may be analyzed in either the Eulerian or Lagrangian frame. A Lagrangian measurement is obtained if the dependent variables are found as a function of the independent variables of time and initial value at $t = 0$. A Eulerian type of measurements describes a dependent variable as a function of the spatial domain. One objective of this study is to quantify the effect of initial conditions on dispersion in a round jet. A range of diameters is considered with droplet response times which encompass the gas time scales.

2. EXPERIMENTAL METHOD

Details of the experimental method are discussed elsewhere by Call & Kennedy (1991) and only a brief description is provided here. A schematic of the experiment is shown in figure 1. A steady stream of droplets is generated using a piezoelectric transducer. The droplets are accelerated by the air flow in the nozzle contraction. As each droplet passes from the nozzle, it intercepts an He–Ne laser beam which is monitored by a photodiode. The diode signal is used as a trigger for the data acquisition system and allows the time-of-flight to be measured for each droplet. As the droplet travels axially downstream, it is radially displaced by the jet turbulence and the displacement from the jet axis is measured with a sheet of laser light and a position-sensitive

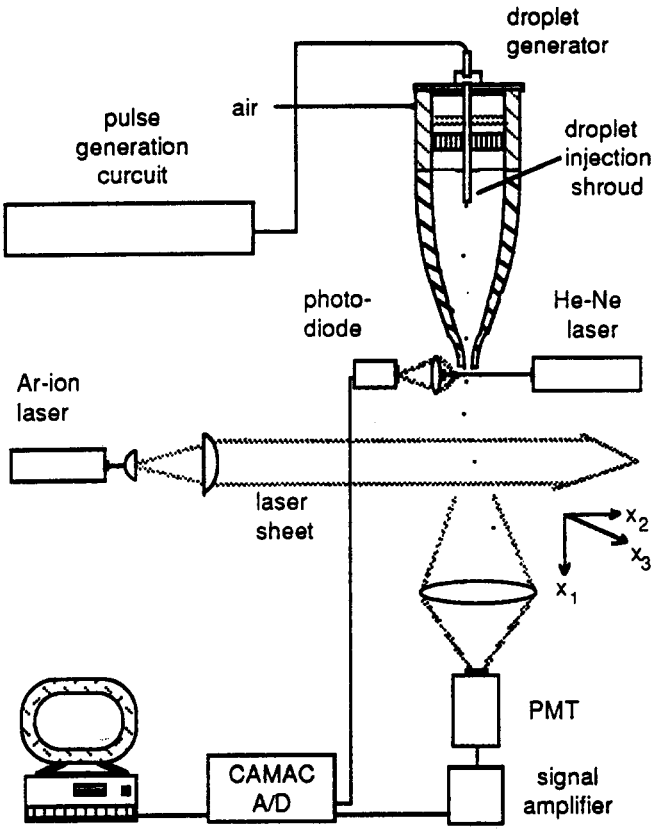

Figure 1. Schematic of the experimental apparatus.

photomultiplier tube. Droplet dispersion statistics are computed from the position measurements. Particle time-of-flight measurements can be differentiated to give mean axial velocity profiles.

For the present air jet, the Reynolds number is 15,000 based on a nozzle diameter of 7 mm. The axial velocity profile of the jet was measured with a hot-wire anemometer and is shown in figure 2. The figure orientation was chosen to facilitate an accurate polynomial curve fit, which is included in the caption. The centerline velocity is 31 m/s and the measured r.m.s. velocity is 0.05 ± 0.02 m/s across the profile.

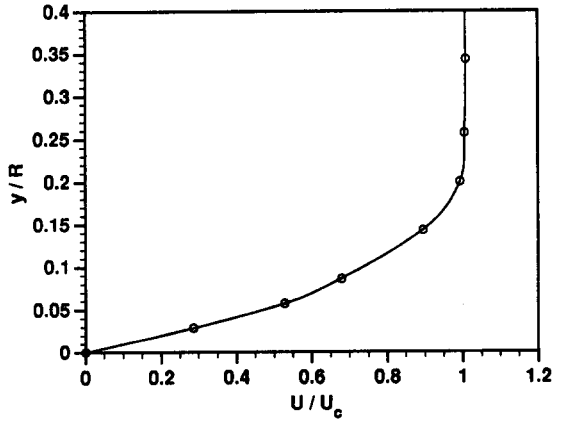

Figure 2. Hot-wire measurements of the velocity profile by the nozzle exit. The distance y from the outer edge of the jet is normalized by the nozzle radius R. The jet axial velocity U is normalized by the centerline value U_C. A curve fit valid for $y/R < 0.3$ is: $U/U_C = -1.373654E + 2(y/R)^4 - 1.211953E + 2(y/R)^3 - 5.225356E + 1(y/R)^2 + 1.168103E + 1(y/R) - 2.536114E - 3$.

The droplet diameter is calculated from measurements of terminal velocity, with an estimated uncertainty of $\pm 2\,\mu$m. This technique has proved reliable in comparisons with microphotography. The droplet size is governed by a nozzle attached to the transducer. The present data for hexadecane droplets cover a range of 35–160 μm. The droplet mass fraction is of the order 10^{-6} and the droplets are separated by more than 1000 droplet diameters; hence, the droplets are non-interacting and have a negligible effect on the gas-phase flow properties. The vaporization of hexadecane droplets in air at 20°C is negligible over the times-of-flight under investigation (typically < 50 ms). Figure 1 illustrates the orientation of the coordinate axes.

As each droplet passes through the sheet an x_2, x_3 displacement pair for each drop is measured. The dispersion in the x_2 or x_3 direction is computed using the following expressions:

$$\sigma^2_{p,x_2} = \frac{1}{n}\sum_{i=1}^{n}(x_{2,i} - \langle x_2\rangle)^2, \quad \sigma^2_{p,x_3} = \frac{1}{n}\sum_{i=1}^{n}(x_{3,i} - \langle x_3\rangle)^2, \tag{4}$$

where n is the number of droplet samples obtained and the x_{2i} and x_{3i} are the measured displacements from the jet axis for each droplet. Since the flow field and dispersion are axisymmetric, $\sigma^2_{p,x_2} = \sigma^2_{p,x_3}$; and since the dispersion is centered about the jet axis, $\langle x_2\rangle$ is numerically close to zero. For experimental dispersion measurements, a total of 1000 droplets are used for statistics at each axial location downstream from the air jet nozzle. The time-of-flight t and x_2, x_3 displacements are recorded for each droplet at a particular axial location x_1.

3. NUMERICAL SIMULATION METHODOLOGY

The dispersion of particles in the turbulent jet has been simulated numerically using a stochastic approach. The flow field was calculated with the Reynolds stress model of Dibble *et al.* (1984), which yielded an Eulerian description of the turbulence statistics. A Lagrangian simulation of the droplet dispersion was then performed in the same manner as Shuen *et al.* (1983) by integrating the equations for particle motion through the flow field. Three equations were used for the force components on a particle with only drag and gravity considered. Three equations for particle velocity were integrated simultaneously with a fourth-order Runge–Kutta scheme to yield particle velocity $\bar{v}_p$ and position $\bar{x}_p$:

$$\frac{d\bar{v}_p}{dt} = -\frac{3\rho_G C_D}{4 d_p \rho_p}(\bar{v}_p - \bar{v}_G)|\bar{v}_p - \bar{v}_G| + \bar{g}, \quad \frac{d\bar{x}_p}{dt} = \bar{v}_p, \tag{5}$$

where the drag coefficient $C_D = 24(1 + Re_p^{2/3}/6)/Re_p$; is the particle Reynolds number based on the droplet diameter d_p, the relative velocity of the droplet and air $|\bar{v}_p - \bar{v}_G|$ and the air kinematic viscosity ν_G. The density of the particle and air are given by ρ_p and ρ_G, respectively. The drag coefficient C_D includes a high Reynolds number correction to the Stokes formula which is important in modeling the behavior of the relatively large droplets. Acceleration due to gravity, $\bar{g}$, is non-zero in the x_1 direction. One thousand particles were simulated to give representative statistics; the integration time step was 1 μs.

The interaction of particles with the turbulence was simulated stochastically by randomly sampling the velocity probability density functions (pdfs), given the mean and variance of each flow velocity component as determined by the second-order closure. The velocity pdfs were assumed to be Gaussian. The typical eddy length and time scales were estimated in the same manner as Shuen *et al.* (1983):

$$L_e = C\kappa^{1.5}/\chi, \quad \tau_e = \frac{L_e}{\sqrt{\frac{2\kappa}{3}}}; \tag{6}$$

κ is the turbulent kinetic energy and χ is the dissipation rate. C is an empirical constant set equal to 0.28 for all simulations. The interaction time for the droplet with the turbulent eddy was taken to be either the eddy lifetime or the transit time for the droplet to cross the eddy, whichever is shorter. The latter quantity was evaluated in the following manner. The distance that a droplet travels is tracked from the beginning of its interaction with an eddy. When this distance becomes

greater than the eddy length scale, the flow velocity pdfs are sampled for new values. For the simulations reported here, the eddy lifetime was usually less than the transit time.

4. RESPONSE TIME SCALES

The dispersion of heavy particles deviates from fluid particles for several reasons, all relating to the particle's inertia. The droplets sizes which have been studied in this investigation cover a large range of response time scales and inertial effects are important. The droplet relaxation time that characterizes the particle inertia is based on the terminal velocity of the particles and is given by

$$\tau_p = \frac{U_T}{g} = \left[\frac{4d_p(\rho_p - \rho_G)}{3C_D\,\rho_G g}\right]^{1/2}, \qquad [7]$$

where U_T is the droplet terminal velocity, g is the gravitational acceleration constant, d_p is the particle diameter, ρ is the density of the particle or gas and C_D is the drag coefficient given in [6], with the Reynolds number based on the droplet terminal velocity. Table 1 shows the scales for the droplets used in this investigation.

Several characteristic time scales have been identified to characterize the gas phase. Wells & Stock (1981) use the Kolmogorov time scale $\tau_K = \sqrt{\nu_G/\chi}$, where ν_G is the gas viscosity and χ is the dissipation rate, and found it to be a useful indicator for the effects of particle inertia. The Kolmogorov scale is characteristic of the smallest time scale of the turbulence and if τ_p is of the same order as τ_K, the droplet can be expected to follow nearly all gas fluctuations. (For our conditions, at $x_1/D = 40$, $\tau_K = 0.6$ ms, and the smallest droplet response time is 3.0 ms.) A second gas time scale, used by Vames & Hanratty (1988) and Hardalupas *et al.* (1989) is given by the Lagrangian gas integral scale defined as $T_f^L = \varepsilon_f/\langle v_f^2\rangle$, where ε_f is the fluid particle diffusivity and $\langle v_f^2\rangle$ is the mean square gas velocity. Shuen *et al.* (1983) estimate a time scale based on a characteristic eddy lifetime given in [6]. This time scale is representative of the larger gas scales, which have the most influence on particle dispersion.

A body force such as gravity can cause a convective shift of the particles relative to the gas, and can result in droplets having a tendency to fall from one region of correlated flow (a turbulent eddy) to another. This phenomenon, referred to in the literature as the crossing trajectories effect, has been shown to be important when the droplet terminal velocity is greater than or equal to the gas r.m.s. velocity. For this investigation, the effect should not be significant since U_T is always less than the r.m.s. gas velocity.

Another effect of inertia relevant to these experiments is related to the droplet velocity response time: a heavy droplet will pass through an eddy if the instantaneous inertial force is considerably larger than the drag force. Due to mean slip between the particles and the flow, the interaction time between a particle and an eddy can be significantly decreased. This inertia effect is related

Table 1. Time scales of the air jet and droplets studied in this investigation

	Droplet diameter (μm)			
	35	60	120	160
Terminal velocity, U_T (m/s)	0.029	0.092	0.27	0.43
Terminal Reynolds, number, $U_T d_p/\nu$	0.07	0.39	2.2	4.76
Response time constant, τ_p (ms)	2.9	9.1	28	44
Turbulence Stokes number, τ_p/τ_e [(a)]	0.16	9.1	1.6	2.4
Kolmogorov Stokes number, τ_p/τ_b [(b)]	4.76	15	45	70
Acceleration Stokes number, τ_p/τ_a				
$x_1/D = 20$: [(c)]	0.17	0.55	1.67	2.63
$x_1/D = 40$:	0.043	0.14	0.42	0.66
Crossing trajectories ratio, $U_T/v_{G,r.m.s}$ [(d)]	0.03	0.1	0.3	0.5
Kolmogorov length scale Ratio, d_p/η_G				
$x_1/D = 20$:	1.38	1.53	3.06	4.08
$x_1 D = 40$:	0.69	0.76	1.53	2.04

[(a)] $\tau_e = 18$ ms, obtained from the jet simulation at $x_1 D = 40$ and [7].
[(b)] $\tau_K = \sqrt{\nu_G/\epsilon} = 0.6$ ms, with ϵ obtained from the jet simulation at $x_1/D = 40$.
[(c)] $\tau_a = 16.7$ ms at $x_1 D = 20$ and 67 ms $x_1/D = 40$.
[(d)] $v_{G,r.m.s.} = 0.90$ m/s at $x_1/D = 40$ on the jet axis from hot-wire measurements.

entirely to mean velocities as opposed to velocity fluctuations and can be particularly important in free shear flows, since the gas mean velocity is continuously decreasing. A time scale characterizing the slip due to acceleration in the gas mean velocity can be defined by the inverse velocity gradient of the gas:

$$\tau_a = |\mathrm{d}\langle U_{p,x_1}\rangle|\mathrm{d}x_1|^{-1}, \quad [8]$$

where $\langle U_{p,x_1}\rangle$ is the mean axial velocity of the gas. τ_a is smallest near the jet exit beyond the potential core of the jet, and increases monotonically as the jet evolves. For our flow conditions: at $x_1/D = 20$, $\tau_a = 0.0167$ s; and at $x_1/D = 40$, $\tau_a = 0.067$ s. Since $x_1/D = 20$, τ_a is of the same order as the turbulence time scale, it should influence the dispersion. At $x_1/D = 40$, this time scale is considerably larger than other scales and becomes unimportant.

Additionally, mean slip can be imposed at the initial condition and sustained over long distances relative to the system geometry. This behavior could be of considerable importance in practical sprays, since much of the droplet mass may be contained in droplets with Stokes numbers >1. Slip should diminish the importance of turbulence on dispersion if the relative velocity is of the order of the gas velocity fluctuations.

The relative importance of inertial effects can be deduced by comparing the ratio of the particle response time to a gas time scale. If this ratio, or Stokes number, is >1, the inertia significantly affects the droplet dispersion. As can be seen in table 1, for our flow conditions and droplet sizes, inertial effects should be important.

The Kolmogorov length scales at $x_1/D = 20$ and 40 for a jet Reynolds number of 15,000 are estimated to be 39 and 78 μm, respectively, using the relations given by Antonia *et al.* (1980). Because the smallest lengths scales of the turbulence are of the same order as the droplet diameters, it is possible that the turbulence may have an influence on the drag which is not predicted.

5. DISPERSION MEASUREMENTS

The radial dispersion of the droplets can be analyzed in either purely Eulerian or Lagrangian terms. The Eulerian dispersion of droplets is shown in figure 3 as a function of the axial location. The dispersion measurements $\sigma^2_{p,x_2}(x_1)$ represent the droplet spread in one direction of the transverse plane of the jet flow. The subscript x_2 will be used henceforth since x_2 and x_3 statistics contain the same information. Note that for all droplet sizes the dispersion begins to increase quite rapidly for $x_1/D > (20 \text{ to } 30)$.

The experimental approach reported here entails the collection of independent droplet samples of x_1, x_2, x_3 and t; and thus, computations of $\sigma^2_{p,x_2}(t)$ and $\sigma^2_{p,x_2}(x_1)$ can be considered separately. After collecting data at finely spaced axial locations along the jet, the data are sorted into narrow bins of time; the width of each bin is given by $\Delta t/t \leqslant \pm 0.04$. The results shown in figure 4 represent Lagrangian measurements of the x_2 particle dispersion. Particle diffusivities, or dispersion rates, can be estimated from the quasi-linear portion of the data. The initial conditions for the simulations and results are summarized in table 2. Estimation of the initial conditions for the mean axial velocity is described in the next section.

The simulations do a reasonable job of reproducing the data, particularly with respect to the particle diffusivity. However, the agreement is not as favorable as other attempts, such as those reviewed in Faeth (1987). The displacement statistics over the first 10 ms of the simulations significantly underpredict dispersion (even though the measured dispersion is small).

Experimentally, early velocity fluctuations could be caused by two effects. Weak turbulence upstream of the nozzle exit could impart a very small random velocity on the droplets which persists down the nozzle and manifests itself as a perturbation on the initial condition. It is also possible that jet structure, i.e. strong vortical motions within the first 10 jet diameters could induce a random velocity on the droplets. The latter includes the dispersive effects of initial conditions at the nozzle exit as well as turbulent dispersion caused by interaction with the spear layer growth in the early stages of the jet evolution. This suggests that either the dynamics of the flow are not fully reproduced by the Reynolds stress closure model and/or the eddy lifetime approach does not accurately reproduce the actual particle velocity autocorrelation. One aspect of the latter point,

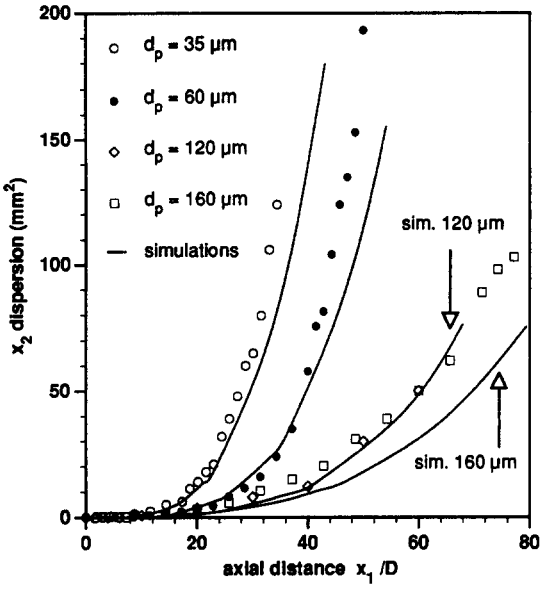

Figure 3. Eulerian dispersion measurements.

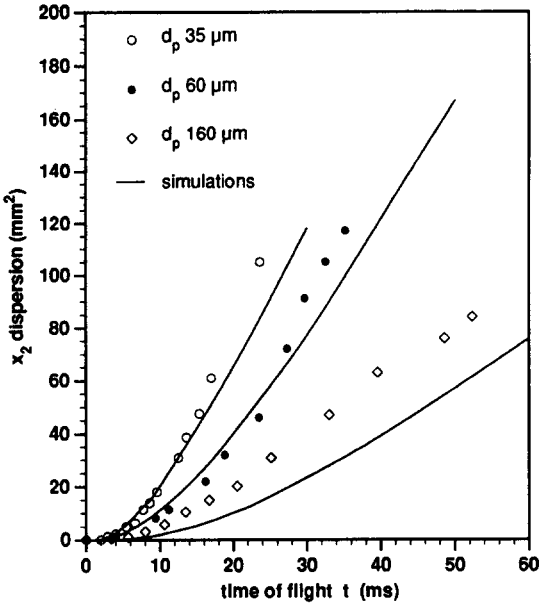

Figure 4. Lagrangian measurements of dispersion.

namely that the eddy lifetime approach should lead to a linear correlation function, was discussed by Berlemont *et al.* (1990). However, both effects are likely to be relevant. Further discussion of the initial conditions is given in section 7.

6. TIME-OF-FLIGHT MEASUREMENTS

Measurements of mean time-of-flight are obtained by ensemble averaging the time each droplet takes to reach a given axial distance. Such time-of-flight measurements are shown in figure 5. The nearly quadratic dependence of time-of-flight on axial position is regarded as consistent with that expected for the round jet configuration as a consequence of the $1/x$ decay in the mean velocity.

For the larger droplet, a hump in the data is observed for very small times (i.e. near the nozzle exit). This behavior is due to the fact that the large droplets significantly lag the flow at the exit. For the first 5–7 nozzle diameters, the droplets are accelerating in the potential core of the jet, where the gas velocity is 31 m/s. Beyond the core, the gas mean velocity drops rapidly, giving rise to an inflection point in the time-of-flight data where the gas and droplet mean velocities are equal. This point occurs near an $x_1/D = 10$. Beyond that point the gas mean velocity is less than the particle mean velocity, giving rise to slip.

The mean velocity profiles for the droplets are easily obtained by differentiating a fifth-order polynomial curve fit of the time-of-flight data and are shown in figure 6. The estimated velocity at $x_1 = 0$, $\langle U_{p,x_1} \rangle_0$, is used as the initial conditions for the simulations. The mean centerline velocity for the gas is shown as a dashed line. These data were obtained using hot-wire anemometry and are in agreement with other measurements of rount jets (e.g. Antonia *et al.* 1980). The mean slip is approximated by the difference between the centerline gas velocity and mean droplet velocity, since the particles are not far from the center, with the exception of the smallest droplets at large

Table 2. Summary of the experimental and numerical results

	Droplet diameter, d_p (μm)			
	35	60	120	160
Droplet axial velocity at the nozzle exit, $\langle U_{p,x_1} \rangle_0$(m/s)	25	21	16.4	13.9
Initial velocity fluctuation for the simulation, $\langle v^2_{p,x_2}(0) \rangle$ (m/s)^2	0.0	0.0	0.0	0.0
Simulated mean square radial velocity at $x_1/D = 40$, $\langle v^2_{p,x_2} \rangle$ (m/s)^2	0.51	0.24	0.076	0.048
Measured particle diffusivity at $x_1/D = 40$, ϵ_{p,x_2} (m^2/s)	0.0059	0.0037	N/A	0.00095
Simulated particle diffusivity at $x_1/D = 40$, ϵ_{p,x_2} (m^2/s)	0.0060	0.0039	0.0014	0.0010

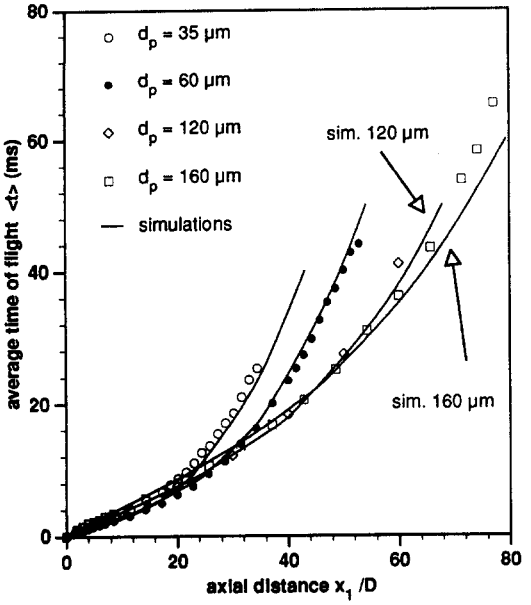

Figure 5. Ensemble-averaged time-of-flight measurements.

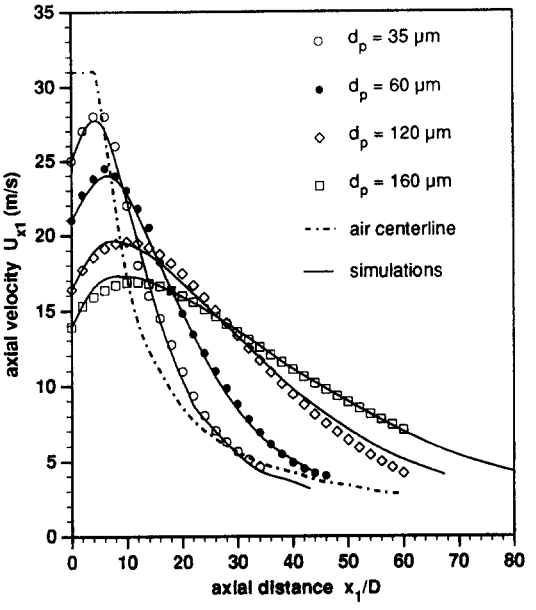

Figure 6. Droplet mean axial velocities.

x_1/D. A typical maximum droplet Reynolds number for a 60 μm droplet with a maximum relative velocity of 5 m/s is $Re_d = 21$; for a 160 μm drop with a relative velocity of 8 m/s, $Re_d = 88$. Recalling the discussion in the previous section regarding the effect of mean slip on droplet–eddy interaction time, it is clear that this inertia effect is dominating the dispersion behavior for droplet sizes >60 μm. The primary cause of slip in our flow is not a consequence of the initial condition for axial velocity *per se*, but rather the slip is due to the rapid negative acceleration of the jet gas which occurs in the first 20 nozzle diameters.

The probability density functions (pdfs) for particle time-of-flight exhibit considerable variation in this type of flow. Figure 7 shows the time-of-flight pdfs for 60 μm droplets at four axial locations in the flow. The average time-of-flight (figure 5) is subtracted from the data so all the pdfs are

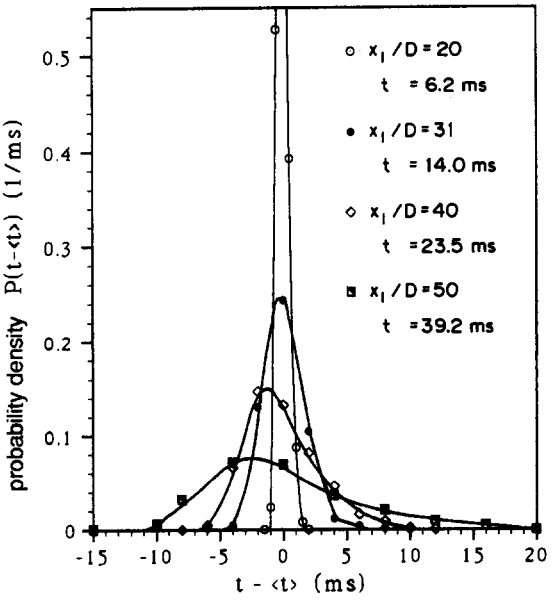

Figure 7. Time-of-flight pdf for 60 μm droplets at four axial locations.

Table 3. Properties of the pdfs for time-of-flight at several axial locations for 60 μm drops

	Axial location, x_1/D			
	20	30	40	50
Mean $\langle t \rangle$(ms)	6.2	14.0	23.5	39.2
Variance $\langle (t - \langle t \rangle)^2 \rangle = \sigma^2$ (ms^2)	0.15	2.45	7.6	33.6
Skewness $\langle (t - \langle t \rangle)^3 \rangle / \sigma^3$	0.54	0.70	0.44	0.25
Kurtosis $\langle (t - \langle t \rangle)^4 \rangle / \sigma^4$	3.2	5.4	2.8	3.1

centered about zero. The average, variance $\sigma_t^2 = \langle (t - \langle t \rangle)^2 \rangle$ and skewness $S = \langle (t - \langle t \rangle)^3 \rangle / \sigma_t^3$ are noted in table 3. Note that all the pdfs have a positive skewness coefficient. At $x_1/D = 20$, the pdf approximates a delta function. As the droplets slow down, the pdfs broaden rapidly, indicating that the droplets are being influenced by the turbulence and some are exposed to regions of the flow where the velocity is not close to the centerline value. This conclusion is consistent with the previous figure, indicating that slip influences the behavior for the first $30x_1/D$ until the droplets equilibrate with the mean flow.

Figure 8 shows the time-of-flight pdfs at $x_1/D = 40$ for four droplet sizes. These data indicate a divergence in the behavior of the two larger droplet sizes from the smaller two. A possible explanation for the observation is that the larger droplet behavior is still influenced heavily by slip and the interaction time with turbulent eddies is limited. The relative velocity for the smaller droplets is of the same order as the gas velocity fluctuations, and thus, slip is less important than turbulence properties. The pdfs are non-Gaussian, having a tail on the positive side.

Additional insight can be gleaned by considering a condition pdf. Figure 9 shows a pdf of droplet axial location conditioned upon the time-of-flight being between $t - \Delta t$ and $t + \Delta t$, where $t = 32.5$ ms and $\Delta t = 1.3$ ms. The pdf is generated by searching the data set at each axial location for samples having the specified time-of-flight. Also shown on the plot's right ordinate is the transverse dispersion σ^2_{p,x_2} of those samples used to generate the pdf. The solid lines were obtained by performing the identical sorting operation on the simulated trajectories. Note that the simulated pdf is more Gaussian and has less variance than the experimental measurements. In general, the variance in time-of-flight (and axial velocity fluctuations) is underpredicted by the simulations. The monotonically decreasing shape of the dispersion data is intuitively reasonable. For a given time-of-flight, the droplets that have not traveled far downstream (low values of x_1/D) have

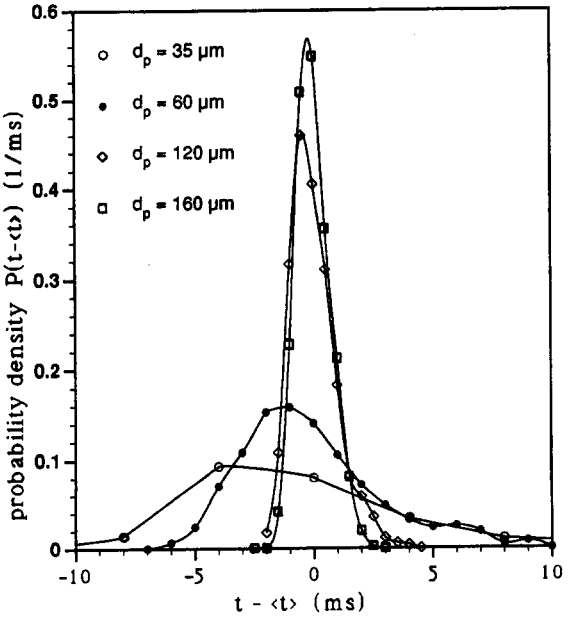

Figure 8. Time-of-flight pdf for four droplet sizes at an axial location of $x_1/D = 40$.

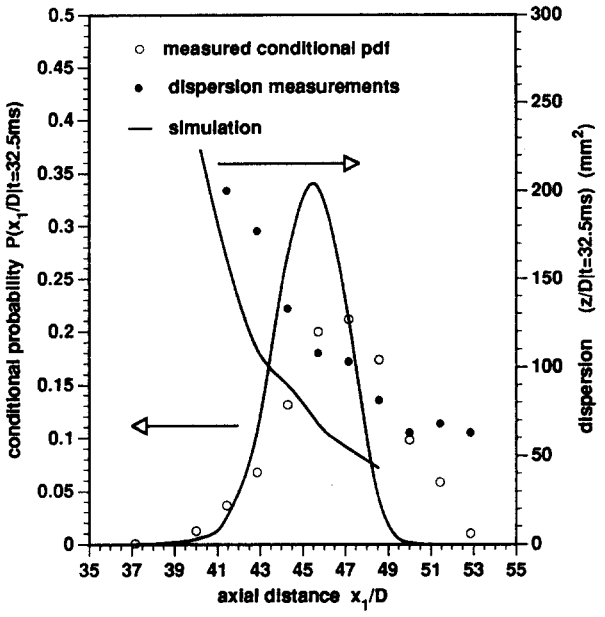

Figure 9. Axial position pdf for 60 μm droplets. The samples are conditioned upon the time-of-flight being near 32.5 ms. The right ordinate shows the dispersion of the conditioned samples.

experienced the outer region of the jet where the mean velocity is lower. Consequently, these samples are characterized by a large value of dispersion. In contrast, the droplets that have traveled far downstream in a given amount of time must have spent more time, on average, near the jet axis where the mean axial velocity was highest.

7. ANALYSIS OF INITIAL CONDITIONS

To enable accurate numerical modeling of the experiments, the initial conditions for the droplets must be well-defined. In addition to the droplets' initial axial velocity, there are two factors which have a measurable influence on the downstream dispersion: initial radial velocity fluctuations; and the initial location of the droplets relative to the jet axis.

The experimental apparatus shown in figure 1 was modified slightly to facilitate investigation of the effects of the initial conditions. The modification involves feeding a very small air flow into the droplet injection shroud (see figure 1). The objective is to slightly perturb the droplets so that a random radial velocity is imparted. Within the contraction, all the droplets are pushed toward the centerline and then exit the jet within $\sim$0.1 mm of the centerline. Their position at the nozzle exit is known to be very near the center since all droplets pass through the He–Ne laser beam which transects the jet axis.

As discussed briefly in the introduction, the initial mean square radial velocity can be estimated using [3]. Paralleling the development of Vames & Hanratty (1988), [1] can be integrated assuming $R^{L}_{p,x_2} = 1$ and $\langle v^2_{p,x_2}(t)\rangle$ is constant and equal to $\langle v^2_{p,x_2}(0)\rangle$ over the short time interval,

$$\sigma^2_{p,x_2} = \langle v^2_{p,x_2}(0)\rangle t^2 \quad \text{(small } t\text{)}, \qquad [3]$$

in order to determine an initial mean square radial velocity $\langle v^2_{p,x_2}(0)\rangle$. In particular, if measurements are made within the potential core of the jet, it may be assumed that any radial velocity is indeed due to initial fluctuations and not shear layer development. This observed initial velocity is statistically imposed on the simulation by giving each droplet in the simulation a unique and random initial velocity with the observed statistical variance. The initial radial velocities are assumed to have a normal distribution with zero mean.

Figure 10 shows this measurement of $\langle v^2_{p,x_2}(0)\rangle$ for the 160 μm droplets in the potential core of the jet. The lower data set A is where no flow was induced to perturb the droplet initial condition

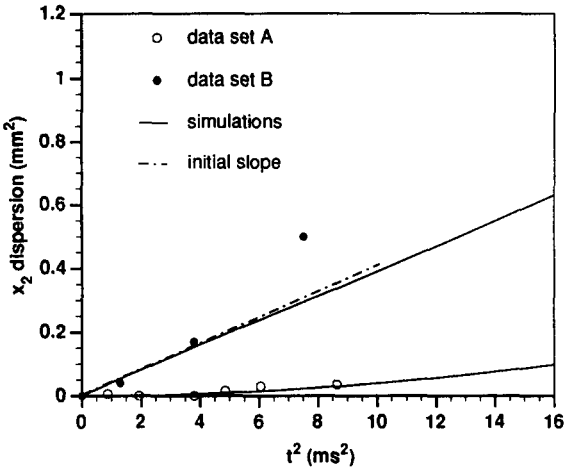

Figure 10. Dispersion data for short time-of-flight. The initial slopes of these data provide an estimate of the radial velocity fluctuation in the potential core of the jet.

and the initial slope is zero. A measurably larger initial velocity fluctuation of $\langle v^2_{p,x_2}(0)\rangle = 0.040$ (m/s)^2 was achieved in data set B with a slight flow in the droplet injection tube. Figure 11 shows the effects of these initial conditions on the downstream dispersion. The simulations show similar trends but underpredict the dispersion in both cases.

An effort was made to investigate the effect of the initial conditions on smaller droplets, but we were unable to generate disturbances in the droplet initial velocities large enough to measure. For droplets with characteristic time scales less than the gas, the droplets equilibrate rapidly; e.g. within 30 jet diameters, regardless of the initial condition. For droplets with characteristic time scales greater than the gas, i.e. $> \sim 90\,\mu$m, the droplets do not equilibrate with the flow and the initial conditions are carried down field, but their impact is slowly damped out.

One would expect that if the droplets are injected slightly off-axis, the dispersion patterns would be affected. In order to determine the effect of a small off-axis perturbation on the dispersion measurements, the apparatus was modified again. By using an extended droplet injection nozzle tip and placing it off-axis, it is possible to force the droplets off-center at the jet exit. The droplets are pushed rapidly toward the centerline by the gas streamlines and the radial pressure gradient in the nozzle contraction. The droplets for the off-axis case were 0.6 ± 0.2 mm off-center at the jet exit. The uncertainty is due to the difficulty in making a precise measurement of the droplet

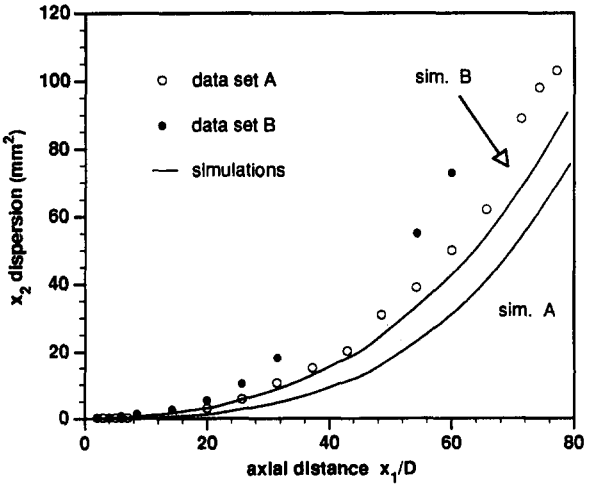

Figure 11. Effect of the initial conditions for 160 μm droplets showing the far-field dispersion.

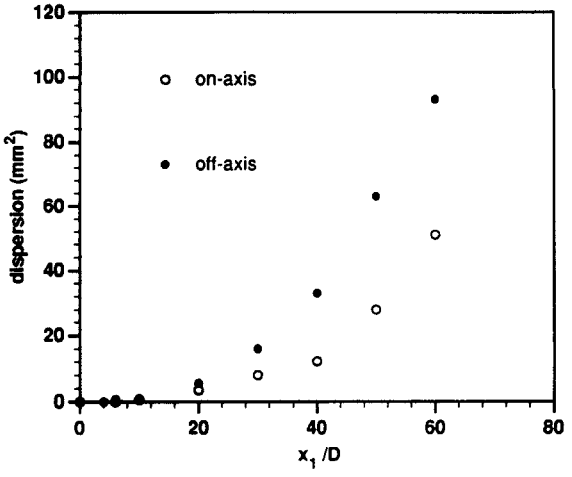

Figure 12. Dispersion measurements for 120 μm droplets illustrating the effect of droplets injected slightly off-axis.

positions relative to the centerline of the jet. In order to produce this perturbation the droplets were released inside the jet near the side wall of the nozzle approx. 70 mm above the jet exit.

As expected, injecting the droplets off-axis has a significant effect on dispersion. Figure 12 shows the measurements for 120 μm droplets injected 0.6 mm off-axis as well as the on-axis base case. In both cases, the droplet displacement is relative to the observed sample mean; i.e. the dispersion is the mean square displacement from the centroid of the droplet distribution. The pdfs of transverse plane displacement become increasingly non-Gaussian as the flow evolves for the droplets injected off-axis, but are essentially Gaussian for the on-axis case.

8. CONCLUSIONS

Particle displacement and time-of-flight statistics have been measured using a particle imaging method developed for this study. The statistics can be cast in a Eulerian or Lagrangian form, since individual particles have been tracked from a known initial location and each particle's time-of-flight is measured. The expreiments have been simulated using a second-order closure for the jet flow and a Lagrangian integration for particle trajectories.

The droplets are far from equilibrium with the turbulence during the first $30x_1/D$ due to mean slip between the particles and gas. The slip is induced by the rapid acceleration of the jet. It decreases the interaction time between the particles and the surrounding gas and leads to decreased dispersion. For large droplets, the effect of the initial conditions at the nozzle exit may persist far downstream. This finding may be important with regard to modeling practical combustion sprays, where up to half of the fuel mass can be contained in droplets with significant inertia.

The radial displacement distributions are Gaussian to within the accuracy of the data, and the measurements of dispersion show the same limiting cases as do measurements from other types of flows. Dispersion grows quadratically in time early in the droplet history, then slows to a nearly linear growth rate. Beyond an axial distance of $x_1/D = 30$, the variance in time-of-flight begins to grow rapidly and is non-Gaussian. The time-of-flight pdfs have a positive skewness, with measured values centered about a value of 0.5. The numerical simulation did not reproduce this aspect of the data, and in general, underpredicted the variance of time-of-flight and axial velocity.

The measured statistics are directly comparable to the droplet dispersion simulations. Simulations of particle dispersion have yielded reasonable agreement with the measurements, particularly for the smaller droplets which have response times less than the gas integral scale. The stochastic simulation underpredicted dispersion for the large droplets and the effect of initial conditions on dispersion has been quantified. It is recommended that velocity autocorrelations be directly measured in jets since such data is needed to further evaluate this simulation methodology.

Acknowledgement—This material is based upon work supported by the U.S. Air Force Office of Scientific Research under Award No. AFOSR-89-0392.

REFERENCES

ANTONIA, R. A., SATYAPRAKASH, B. R. & HUSSAIN, A. K. M. F. 1980 Measurements of dissipation rate and some other characteristics of turbulent plane and circular jets. *Phys. Fluids* **23,** 695–699.

BERLEMONT, A., DESJONQUERES, P. & GOESBET, G. 1990 Particle Lagrangian simulation in turbulent flows. *Int. J. Multiphase Flow* **16,** 19–34.

CALL, C. J. & KENNEDY, I. M. 1991 A technique for measuring Lagrangian and Eulerian particle statistics in a turbulent flow. *Expts Fluids* **12,** 125–130.

CHEN, P. P. & CROWE, C. T. 1984 On the Monte-Carlo method for modelling particle dispersion in turbulent gas–solids flows. *ASME FED (Energy Resour. Tech. Conf.)* **10,** 37.

CROWE, C. T., CHUNG, J. N. & TROUTT, T. R. 1988 Particle mixing in free shear flows. *Prog. Energy Combust. Sci.* **14,** 293–345.

DIBBLE, R. W., KOLLMANN, W. & SHEFER, R. W. 1984 Measurements and predictions of scalar dissipation in turbulent flames. In *Proc. 20th Symp. (Int.) Combust. Inst.*, pp. 345–352.

FAETH, G. M. 1987 Mixing and combustion in sprays. *Prog. Energy Combust. Sci.* **13,** 293–345.

GOSMAN, A. D. & IOANNIDES, W. 1981 Aspects of computer simulation of liquid fueled combustion. AIAA Paper No. 81-0323.

HARDALUPAS, Y., TAYLOR, A. M. K. P. & WHITELAW, J. H. 1989 Velocity and particle-flux characteristics of turbulent particle-laden jets. *Proc. R. Soc. Lond.* **A426,** 31–78.

SHUEN, J.-S., CHEN, L.-D & FAETH, G. M. 1983 Evaluation of a stochastic model of particle dispersion in a turbulent round jet. *AIChE Jl* **29,** 167–170.

SNYDER, W. H. & LUMLEY, J. L. 1971 Some measurements of particle velocity autocorrelation functions in a turbulent flow. *J. Fluid Mech.* **48,** 41–71.

SOLOMON, A. S. P., SHUEN, J.-S., ZHANG, Q.-F. & FAETH, G. M. 1985a Structure of nonevaporating sprays, part I: initial conditions and mean properties. *AIAA Jl* **23,** 1548–1555.

SOLOMON, A. S. P., SHUEN, J.-S., ZHANG, A.-F. & FAETH, G. M. 1985b Structure of nonevaporating sprays, part II: drop and turbulence properties. *AIAA Jl* **23,** 1724–1730.

TAYLOR, G. I. 1921 Diffusion by continuous movements. *Proc. Lond. Math. Soc.* **20,** 196.

VAMES, J. S. & HANRATTY, T. J. 1988 Turbulent dispersion of droplets for air flow in a pipe. *Expts Fluids* **6,** 94–104.

WELLS, M. R. & STOCK, D. E. 1983. The effects of crossing trajectories on the dispersion of particles in a turbulent flow. *J. Fluid. Mech.* **136,** 31–62.

YUU, S., YASUKOUCHI, N., HIROSAWA, Y. & JOTAKI, T. 1978. Particle turbulent diffusion in a dust laden round jet. *AIChE Jl* **24,** 509–519.